GE8-32668 MD

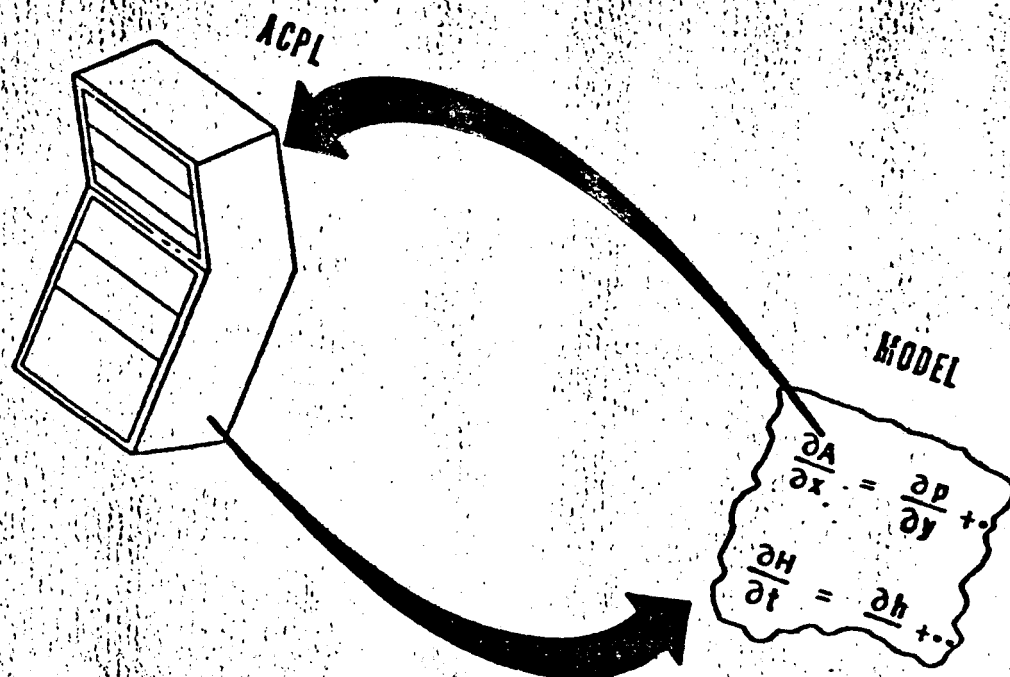# ATMOSPHERIC CLOUD PHYSICS LABORATORY (ACPL) SIMULATION SYSTEM

MATHEMATICAL DESCRIPTION

(NASA-CR-183775) ATMOSPHERIC CLOUD PHYSICS
LABORATORY (ACPL) SIMULATION SYSTEM
MATHEMATICAL DESCRIPTION (GE) 42 p

N90-70090

00/47   Unclas   0235596

$$\frac{\partial A}{\partial x} = \frac{\partial p}{\partial y} + \cdots$$

$$\frac{\partial H}{\partial t} = \frac{\partial h}{\partial t} + \cdots$$

GENERAL *GE* ELECTRIC

Date of Change	Pages Affected
June 27, 1980 *WDB*	Incorporated Phase II Simulation. Revised Table of Contents and Introduction. Changed Bibliography from Section 9 to Section 11. Added Sections 9 and 10, Appendices F and G. Replaced Appendix E.

Supersedes page ii, original issue

TABLE OF CONTENTS

New page

SECTION 1 - INTRODUCTION

This document describes the mathematical formulation of the Phase I and Phase II models of the cloud chambers included in the Atmospheric Cloud Physics Laboratory (ACPL). We shall assume that the user is reasonably familiar with the ACPL facility, and with the operating principles and functions of the cloud chambers included therein. The Phase I models of these cloud chambers are simplified models which assume ideal chamber geometries and operating conditions. The goal of the Phase I simulation program has been to provide models which permit the Principal Investigators for the first ACPL flight to study the essential physical features of their proposed experiments. In the Phase II simulation is the modification of the SDL and CFD models to allow aerosol particles and cloud droplets to move across the chambers in response to phoretic focus created by gradients in gas temperature and composition. Details of hardware design or the departures from ideal conditions which will be present in any real experimental system are not included in Phase I or Phase II.

In Section 2, we summarize briefly the types of experiments to be performed with the ACPL cloud chambers. Section 3 describes the different types of models required by these experiments. A qualitative summary of the physical processes involved in these models is given in Section 4. In Section 5, we derive a general formulation of the physical problem which can be adapted to each of the Phase I models. Sections 6, 7, and 8 describe the actual formulation used for the adiabatic expansion chamber, the non-adiabatic expansion chamber, respectively. We do not go into the numerical methods used in any detail. They will be mentioned from time-to-time, however, because there are several points at which the mathematical formulation was chosen for computational reasons. Section 9 begins the description of the Phase II models and describes the SDL and CFD models with phoretic and gravitational motion of aerosols and droplets.

Supersedes page 1-1, original issue

SECTION 9 - SDL AND CFD MODELS WITH PHORETIC AND
GRAVITATIONAL MOTION OF AEROSOLS AND DROPLETS

The preceding sections have described the formulation of the Phase I ACPL Cloud
Chamber Models. The present section begins the description of the Phase II
models. The first two tasks in the Phase II simulation program were the modification
of the SDL and CFD models to allow aerosol particles and cloud droplets to move
across the chambers in response to phoretic forces created by gradients in gas
temperature and composition and, optionally, in response to gravitational forces.
These models were developed in response to the needs of the planned experiments
on SDL-CFD comparisons in both zero-g and one-g environments, and on phoretic
motion of aerosols in the CFD.

The basic model equations developed in Section 5 include an equation for the
movement of particles with the gas in the ACPL chambers (eq. 5-2-9). However, as
stated in Section 7, early attempts to follow motions of cloud droplets in the
Phase I models gave physically unrealistic results, so they were deferred at that
time. The problem was basically that the numerical method used gave rise to
non-physical artifacts in the results. It has turned out that extensive changes
in the computer programs were required to avoid such artifacts.

Section 9.1 below presents the equations used to compute aerosol/droplet
velocities. Section 9.2 describes the computational techniques employed to
follow the particle motion. Finally, Section 9.3 describes some other features
of these new models which differ from the Phase I models.

9.1 EQUATIONS OF PARTICLE/DROPLET MOTION

9.1.1 Mechanisms of Particle Motions

Four different causes of particle motion are included in these models: motions
due to the fact that the gas itself is moving; motions due to temperature gradients
(thermophoresis); motions due to concentration gradients in the gas (diffusio-
phoresis); and motions due gravity forces. In this discussion, we are concerned
only with the component of particle velocity in the Z-direction (the coordinate
normal to the chamber plates in both the SDL and CFD models) which we denote w_p.
Motions parallel to the chamber plates (e.g., the u-component of the velocity
in the CFD due to the gas flow through the chamber) are already included in the

Replaces page 9-1, original issue

models and need no further discussion here. We assume that the particle velocity w_p can be written as:

$$w_p = w + w_T + w_D + w_g \tag{9-1}$$

where w is the molar average gas velocity in the Z-direction (discussed in Section 4-2), and w_T, w_D and w_g are the velocity components due to thermophoresis, diffusiophoresis, and gravity, respectively. Each of these components is treated separately in the following.

9.1.2 Gas Motions

A net flux of gas molecules in the Z-direction can arise from temperature changes, diffusion of one component of the gas with respect to another, and changes in the total amount of gas present in the system due to condensation or evaporation of water. This w-component of gas velocity is already computed explicitly in the Phase I CFD model (eq. 8-18), but not in the SDL model. What is computed in the Phase I SDL model is the change in volume of each grid cell, from which the displacement in position of the cell boundaries with time is easily determined. A simple subroutine, which computes the flow velocity in each cell as the average of the velocities at its two boundaries, has been added here.

9.1.3 Thermophoresis

We use the thermophoretic velocity equation of Dejaguin and Yalamov, which is quoted by Goldsmith and May in Davies' book, <u>Aerosol Science</u> (1966). The equation is

$$w_T = -\frac{2}{3} \cdot \frac{8k + k_p + 2C_{tr}\frac{\ell}{r_p}k_p}{2k + k_p + 2C_{tr}\frac{\ell}{r_p}k_p} \cdot \frac{k}{5p} \frac{dT}{dZ} \tag{9-2}$$

in which the symbols are defined as follows:

  k = thermal conductivity of the gas
  k_p = thermal conductivity of the particle
  r_p = particle radius
  ℓ = molecular mean free path in the gas
  p = gas pressure
  T = gas temperature

Replaces page 9-2, original issue

The coefficient C_t is defined by the equation

$$C_t = 15(2-\alpha)/8\alpha$$

where α is the thermal accommodation coefficient of the particle, a parameter which is set by the user as part of the input to all the ACPL models. Since most of the particles of interest in the ACPL experiments are dilute solution droplets, we have used the thermal conductivity of water for k_p. The mean free path of an air molecule is calculated from the equation

$$\ell = 0.0225T/p \tag{9-3}$$

where p is in dynes/cm^2 and T is in degrees K.

The Dejaguin-Yalamov equation is one of a fairly large number of possible equations. A search of the literature shows clearly that a uniformly successful theory of thermophoresis, applicable to all sizes and types of particles, has yet to be developed. The main problem arises in the determination of the thermophoretic velocity of particles which are large in comparison with the molecular mean free path in the gas. Different theoretical treatments diverge considerably in this particle size region. Unfortunately, the available experimental data also show considerable scatter. The Dejaguin-Yalamov equation appears to be as good as any for water droplets, judging from the results presented by Goldsmith and May; hence its use here.

9.1.4 Diffusiophoresis

To a first approximation, the diffusiophoretic velocity is independent of particle size and depends only on the ratio of molecular weights of the diffusing gases. The equation for the diffusiophoretic velocity used here is

$$w_D = - \frac{(1-\epsilon^{\frac{1}{2}})D\nabla X_a}{X_a(1-\epsilon^{\frac{1}{2}}) + \epsilon^{\frac{1}{2}}} \tag{9-4}$$

where $\epsilon = M_v/M_a$, the ratio of the molecular weights of water and air, X_a is the mole fraction of air, and D is the coefficient of diffusion of water vapor in air.

New page

9.1.5 Gravitational Settling Velocity

The models allow the user to turn the gravitational force on or off, for simulation of either one-g or zero-g experiments. The gravitational settling velocity equation used here is

$$w_g = \frac{2}{9} \cdot \frac{\rho_\ell \, g r_p^2}{\eta} (1 + A \frac{\ell}{r_p}) \qquad (9\text{-}5)$$

where ρ_ℓ is the density of the particle (taken here as the density of liquid water), g is the gravitational acceleration, η is the viscosity of air, and A is a coefficient defined by the equation

$$A = 1.008 \ (2-\alpha)/\alpha.$$

When the gravity term is included in the models, it is assumed that the chambers are operated with the plates horizontal and with the top plate warmer than the cold plate to insure stable stratification of the gas in the chamber.

9.2 NUMERICAL TREATMENT OF DROPLET MOTION

In the Phase I models, water droplets were labeled by two parameters: their location, i.e., the index of the grid cell in which they were located; and the size, or more precisely, the critical supersaturation, of the aerosol particles on which they were formed. Droplets formed on a given nucleus size class were assumed to be uniformly distributed throughout a given grid cell. The first (unsuccessful) attempts to follow droplet motions in these models used a two-step numerical process. In the first step, any motion of gas across a cell boundary carried with it a corresponding number of droplets. In the second step, a new mass-averaged droplet radius was calculated for each class of particles in each cell. That is, the liquid water content in each cell and for each nucleus size class was redistributed among droplets so that (a) all droplets were assigned the same radius, and (b) the total number of droplets and the total mass of liquid water were conserved.

The second of these steps, the size-averaging process, gave results which often made no physical sense. A brief discussion of the reasons why this approach did not work will help to lay the groundwork for the approach used in the Phase II models. In a diffusion chamber model, the supersaturation varies considerably

from one grid cell to another. Thus, nuclei of a given critical supersaturation
can be activated in one cell and not in an adjacent cell. Once activated, drop
growth is rapid, leading to a large difference in droplet size between cells.
That is, in one cell, droplets would be growing rapidly on a given class of
nuclei, while in the adjacent cell only small haze droplets would be present.
The difference in droplet radius in such a situation can easily be a factor of
10, corresponding to a factor of 1000 in droplet mass. Now, if we transfer only
one such large droplet across a cell boundary, it carries with it enough liquid
water to double the mass of 1000 haze droplets in the second grid cell when the
droplet masses are averaged. In many cases, such mass increases were sufficient
to raise the average droplet size in the second cell above the critical radius,
so that all the droplets in that cell would begin to grow, even though the
supersaturation in that cell had never reached the critical supersaturation for
that class of nuclei. This of course is physical nonsense. As a result, aerosol
and droplet motions were omitted from the Phase I models, as stated in Section 7.

It is obvious that one must avoid the numerical process of "mixing" droplets
with different histories and then averaging their sizes. One impractical way to
do this is to keep a separate record of each group of droplets that crosses a
cell boundary. The problem here is that the number of droplet groups increases
very rapidly with time, and the computer memory and time required would soon
exceed the capacity of any known computer. The approach taken here was to keep
a record of the "center of mass" of each droplet group, and to move the entire
group from one cell to another when its center of mass crossed the boundary.
Numerically, this is equivalent to a suggestion made to the author by Prof. Wm. Scott
of the University of Nevada at Reno, that each group of droplets be assigned a
specific vertical location (i.e., do not assume that the droplets are uniformly
distributed within a cell, but rather that they are spread out horizontally in
a layer of infinitesimal thickness so that all the droplets in a group will cross
a cell boundary at the same time). The droplet groups are labeled by their
location at the beginning of the simulated experiment (i.e., by the index of
the grid cell in which they started) and by their nucleus size class. In
addition to the droplet radius and number concentration, one must now also
keep a record of the vertical position in the chamber (the Z-coordinate) and
the migration velocity of each group. At the beginning an an SDL run, or at
the time of sample injection into the CFD, the droplet groups are positioned

New page   9-5

at the midpoints of their respective grid cells. Droplets or haze particles
are removed completely from the system whenever the center of mass of a group
reaches one of the chamber plates.

There undoubtedly are other good approaches to this problem. The approach taken
here has two advantages: it is conceptually straight-forward, and it works.
Especially when the gravitational force is "turned on", the model shows how
droplets of different sizes move through the grid at different rates and
eventually impact the chamber plates. Implementation of this approach did
involve a fairly extensive modification of the code from the Phase I models,
however, because of the need to carry the extra variables mentioned above for
each droplet group, and the need to determine the current position of each
group in calculating droplet growth rates, migration velocities, liquid water
contents, etc. at every time step.

9.3 OTHER FEATURES OF THE MODELS

The Phase I SDL model used an explicit difference scheme to solve the heat
conduction and vapor diffusion equations. Use of explicit difference methods
for differential equations always limits the size of the time step that can
be used, to avoid numerical instability. Section 7 mentioned that an SDL
model using an implicit, unconditionally stable difference scheme had also
been developed. The Phase II SDL model is based on the latter. The additional
computation time required for the droplet motion calculations would have
substantially increased the running time of a model using an explicit difference
scheme and a small time step.

The Phase I CFD model, on the other hand, required no modifications in this
respect.

The output from both the SDL and CFD models developed during Phase II has been
substantially changed from that furnished with the Phase I models, especially
with regard to the presentation of droplet size information. The Phase II
models still offer a table of temperature, supersaturation, and vapor and
liquid mixing ratios vs. position in the chambers. They also offer the option
of a much condensed output presentation, giving only the temperature

New page

and supersaturation at the median plane of the chamber. There no longer is a printout of the size of the droplets formed on each size class of aerosol particles in each grid cell in the model. The reason for this is simply that, once droplet motions are allowed, it is possible for a given grid cell to contain droplets of comparable size, but formed upon nuclei of different sizes which originated in different parts of the chamber. In short, differential movements of the droplets can result in a thorough "scrambling" of the original nuclei distribution in space. The printout now consists of a table of the number concentration of droplets in different size ranges as a function of position in the chamber, without regard to the nuclei on which they were formed. The droplet size spectrum uses size (radius) intervals of 0.2 μm below 1 μm, 0.5 μm intervals from 1 to 5 μm, and 1 μm intervals from 5 to 10 μm. Again, the user has the option of omitting this table printout if desired, and printing only the total flux of activated droplets in the case of the CFD, or the total number of activated drops per square centimeter of plate area in the case of the SDL.

These Phase II SDL and CFD models in effect supplant the corresponding Phase I models. They give a more accurate simulation of the processes taking place in these cloud chambers and offer more options to the user. Anyone using the Phase I models should consider switching over to these models.

New Page

SECTION 10 - TWO-DIMENSIONAL SDL MODEL

Previous SDL models used only a single space dimension, the coordinate normal to the chamber plates (here labelled the Z-coordinate). In other words, these models assumed that gradients in the values of all variables in the coordinate parallel to the chamber plates were negligible. For studies of droplet formation on a uniformly distributed aerosol, in regions away from the edges of the chamber plates, this assumption introduces little error. However, experiments have now been proposed which depend essentially on the effects of gradients in the radial coordinate. These experiments are of two basic types. In the first type, a single ice particle will be grown near the center of the chamber. In the second, a "thermal probe", whose temperature can be varied independently of the chamber plate temperatures, will be inserted into the center of the chamber. This section describes a two-dimensional axisymmetric model of an SDL chamber, which represents the first step in the development of a capability to simulate such experiments.

The model describes a cylindrical section of the SDL chamber, bounded on its upper and lower surfaces by the chamber plates, and centered on the axis of symmetry of the chamber. It is an axisymmetric model; angular variations are neglected. The coordinate normal to the chamber plates is again the Z-coordinate. The primary difference between this model and previous SDL models is the numerical approach to solution of the heat conduction and vapor diffusion equations in these coordinates. Droplet nucleation and growth are treated exactly as in earlier models. The model provides for insertion of a cylindrical thermal probe concentric with the axis of symmetry. A model of ice particle growth has not yet been incorporated in the program.

Section 10.1 outlines the formulation of the model. Numerical methods are very briefly described in Section 10.2. Finally Section 10.3 discusses some additional features, and some limitations of the model in its present form.

10.1 TWO-DIMENSIONAL MODEL FORMULATION

This model is based on the same equations (described in Section 5) as were used for the previous models. The difference is that the two-dimensional axisymmetric forms of the gradient and divergence operators are used.

New page

Two of the simplifying assumptions used in the Phase I SDL model are again used here. The first simplification is the neglect of the last term in the full heat conduction equation (5.2.19), for the same reasons as given in Section 7. The second simplification is that motions of aerosol particles and water droplets are not permitted. Incorporation of aerosol/droplet motions in a manner analogous to the Phase II SDL model would involve a substantial additional programming effort (the problem is more complicated in two dimensions than in one) and would also increase both the computer memory requirements and the program execution time. Droplet motions could be added at a later time if desired. Prohibition of droplet motions restricts the model to simulation of zero-g experiments.

A further simplification is that the temperature dependences of the thermal conductivity of air and the coefficient of diffusion of water vapor in air are neglected. This results in a considerable simplification of the program and, again, a reduction in computer memory and time requirements. This simplification could also be removed at a later date if desired.

The user has control over the dimensions of the region to be modeled: the chamber plate separation, and the inner and outer radius of the region to be modeled. He also has control over the spatial resolution in both coordinates, by setting the number of grid points in each direction (NSPACE and MSPACE for the Z and X-coordinates, respectively). The model allows NSPACE and MSPACE to be as large as 21 and 41, respectively. Thus there can be as many as 21x41=861 grid points in the model.

In the Z-direction, the boundaries are the chamber plates. The temperature and water vapor pressure at each plate can vary with time, but in the model as now set up they do not vary with X. Thus at each instant in time the temperature is everywhere constant on each plate.

The boundary condition at the outer radial boundary (M=MSPACE) is that radial gradients are zero, so that there is no flux of mass or energy across this boundary.

The model allows the user to set MMIN, the lower limit of the radial space index M, to a value greater than 1. When MMIN is greater than 1, the model inserts a

New page

solid cylinder of radius (MMIN-1)DX (where DX is the radial grid spacing) concentric with the chamber axis, to simulate a thermal probe experiment. The surface temperature of this solid cylinder is independently controlled by the subroutine TPROBE. The user can insert any desired code in subroutine TPROBE to control the probe temperature at each grid point in the vertical (Z) direction as a function of time. The code provided in the model is just one example of how this might be done.

If MMIN=1, there is no thermal probe, subroutine TPROBE is not called, and the chamber is assumed to be completely filled with gas. The boundary condition at M=1 (X=0) is that all radial gradients are zero. In the model as it now stands, since horizontal gradients vanish at both radial boundaries and at the chamber plates, there is no variation in any variables in the X-direction. The model thus reduces, in effect, to a one-dimensional model. However, this will no longer be true when a growing ice particle is inserted at X=0.

The model simulates the following type of experiment. Initially, both chamber plates are at temperature TZERO. The gas inside the chamber is at temperature and vapor equilibrium with the plates and is at pressure PZERO. The chamber is held at constant volume (i.e., the intake and outlet valves are closed) throughout the experiment. For an initial period of TMRAMP seconds, the top and bottom plate temperatures TW1 and TW2 change at rates DTW1 and DTW2 deg/sec, respectively. Thereafter, both plate temperatures are held constant. All subsequent changes in the properties of the gas and cloud droplets in the chamber are due to the growth of droplets in the supersaturation field and to the effects of the changing temperature of the thermal probe.

10.2 NUMERICAL METHODS

The model is formulated in Lagrangian coordinates, as was the case for previous SDL models. The region to be modeled is initially subdivided into volume elements centered on the grid points, which are equidistant from one another in each of the X and Z directions (although the grid spacings in the X and Z directions can differ from one another). In each time step, the boundary surfaces between the volume elements move with the mean molar velocity of the gas, so that there is no net flux of matter across any boundary (except at the chamber plates,

which are fixed in space and thus are not true Lagrangian surfaces). Thus the
total number of moles of matter (air plus water vapor plus liquid water) in each
volume element is exactly constant during each time step. As described in Section
7, this approach eliminates the mean molar gas velocity from the equations, and
the remaining equations are linear. As in the previous models, this approach
also requires a subsequent numerical operation to restore the boundaries to
their original positions after each time step. This operation is carried out
by shuffling matter and energy between cells so as to conserve the total energy
and the total mass of each substance in the chamber.

The model first computes the growth of cloud droplets and the resultant changes
in the concentration of liquid and vapor in each cell. The diffusion of air
and water vapor between cells is then computed, followed by the solution of the
temperature (heat conduction) equation. The major problem encountered in the
development of this model was the selection and implementation of algorithms
to solve the diffusion and temperature equations in two dimensions. This
problem is more critical in two-dimensional than in one-dimensional models
because (a) the added dimension increases the complexity of the difference
equations at each grid point, and (b) the number of grid points is increased
by at least an order of magnitude. The method chosen here is the "alternating-
direction-implicit" (ADI) algorithm. As its name indicates, this algorithm
alternates back and forth between two sets of difference equations in successive
time steps. In one step, it treats the X-component of the Laplacian operator
in the diffusion or heat transfer equation implicitly and the Z-component
explicitly; in the next step it reverses the roles of the two coordinates. In
an explicit difference equation, the second derivative in the Laplacian is
determined from a finite-difference operator involving the values of the
dependent variable at the beginning of the time step, which are known. In an
implicit equation, the values of the variable at the end of the time step, which
are the unknown values we are solving for, are used. Since the finite-difference
form of the second derivative requires the values of the variable at the grid
point and its nearest neighbors on each side, each implicit equation contains
three unknowns. For many two-dimensional problems, the ADI algorithm is the
most efficient computational method in terms of both computer time and memory.

New page

It is unconditionally stable, so that any size time step can be used. (It is still true that the accuracy of the solution improves as the time step decreases.)

The main disadvantage is that separate codes must be written for each "direction", which doubles the probability of programming errors and the time spent debugging the program. The equations corresponding to each grid point must be re-ordered for the two directions; the implicit-X algorithm solves them one row at a time, while the implicit-Z algorithm solves them one column at a time.

The diffusion equation, whose finite-difference form is derived exactly as in Section 7, equations 7.2 through 7.6, gives rise to a set of simultaneous linear algebraic equations whose coefficient matrix is tridiagonal. Solution of such an equation set is very rapid, even for the large equation set generated by a two-dimensional model. The temperature equation for constant-volume chamber operation is considerably more complicated, because the temperature change at each grid point depends on the change at every other grid point, as shown by equations 7.7 and 7.9. In other words, the coefficients are non-zero in every term for every grid point, giving a set of hundreds of equations in hundreds of unknowns. Solution of such an equation set is out of the question for even the largest, fastest computers. Fortunately, a transformation of variable was found which greatly simplifies this system. Defining a new variable $\theta = NT$, where N is the number of moles of gas (air plus water vapor) in each volume element and T is the temperature, and then subtracting one such equation from all the others, gives an equation set whose coefficient matrix is zero everywhere except on the tridiagonal elements and in one row and three columns. This set is somewhat more complicated to solve than a tridiagonal system, but immensely simpler and more economical than solving a full n x n system where n can be as large as 861.

In the model, the ADI algorithm is solved in both directions before carrying out the shuffling operation to restore the original volume elements. In a two-dimensional model, there is no unique way to do this shuffling without explicitly solving an equation of motion for the gas in the chamber. Because the shifts in the positions of the boundaries between cells are always quite small, it was felt that the added effort required to solve an equation of motion in two dimensions was not justified. It was thus decided to first restore the

New page

vertical cell boundaries, by shuffling matter and energy horizontally between cells, and subsequently to carry out the corresponding operations in the perpendicular direction. This solution is not unique; reversing the order of these two steps would give slightly different results. The differences, however, are second-order quantities in the cell boundary displacements and are thus very small when the displacements themselves are small.

10.3 OTHER COMMENTS

The user of this model will soon notice four significant features; (1) its use will require more direct participation on his part; (2) it requires a lot of computer memory; (3) it uses up a lot of computer time; and (4) it produces a lot of numerical output.

The first feature is in many ways a result of the last three, but not entirely. Previous ACPL models were designed to simulate a relatively well-defined set of experiments. The two-dimensional SDL model, on the other hand, is designed to make it possible to simulate new experiment concepts, such as the thermal probe concept, for which the experiment parameters are far less well defined. Thus at the very minimum, the user will have to experiment with the code in subroutine TPROBE to see what experimental parameters, if any, will give the desired class of results. At the same time, the model was designed so that eventually an ice crystal growing between the chamber could be simulated, without having to develop an entirely new model from the ground up. It is by no means clear that an "accurate" model of ice crystal growth can be devised without some iterative interactions between laboratory results and model formulations.

The program in its present form requires between 40K and 50K words of computer memory; the exact number will vary from one computer to another. This number could easily have been much larger; a number of steps were taken to keep the memory requirements down. For instance, a blank COMMON block was used so that several variables, needed at different times in different subroutines, could share the same memory locations. The preceding sections have noted several simplifying assumptions which had, as at least one result, the effect of reducing memory requirements. However, there is one further limitation in the

New page

model that has a larger effect: a maximum of 10 nuclei/droplet classes is available to characterize the condensation nucleus spectrum. All previous models allowed up to 100 nuclei size classes to give a high-resolution critical supersaturation spectrum. This means that 100 memory locations had to be reserved for each grid point in these models. Had this also been done in the two-dimensional model, it would have required 86,100 words in memory for the nuclei/droplet population alone. If the user desires higher resolution than 10 classes for the two-dimensional model, he can increase the first dimension of all the variable arrays in COMMON block ARAY2D.

The computer-time requirements are related to the comments in the preceding paragraph. Computation time goes up as the number of grid points and the number of droplet classes increase, and as the time per step decreases. Unfortunately, the "accuracy" of simulation decreases as steps are taken in any one of these areas to reduce program execution time. For each type of experiment simulation, it would be desirable for the user to try different values of the grid spacing and the time step, to find his own optimum trade-off between accuracy and execution time. (By this we mean that a high-resolution grid and a small time step should give a fairly accurate approximation to the solution of the <u>differential</u> equations; if a somewhat coarser grid and larger time step give results sufficiently close to this "accurate" solution, the user may find this an acceptable compromise.)

The problem of the sheer volume of numerical output is, in the writer's opinion, the biggest problem of all. For the one-dimensional models, it was possible to print out a single table giving the values of temperature, supersaturation, liquid water content, etc., at each grid point at reasonable time intervals. Only when droplet size information for polydisperse nuclei distributions was desired, was it necessary to go to a separate table of output for a single variable. For the two-dimensional model, on the other hand, a table of up to 21 columns and 41 rows is required to list the output for a single variable such as temperature, and a print-out of droplet size information will take up so much space and present so many numbers as to be virtually incomprehensible. In short, the writer feels that line printer output from this model is of little use except to show in a very gross way how the results change with time or variations in input parameters.

New page

The only resolution to this problem is to use computer-generated graphics.
Unfortunately, computer graphics programs are generally not transportable from
one computing system to another. Each user will thus probably find it necessary
to add his own graphics output routines to this model. For displaying two-
dimensional data, the optimum graphics output format is the use of contour plots
or, perhaps a little less satisfactorily, three-dimensional surfaces to display
the variation of each variable vs both X and Z at each instant in time. Routines
to generate either of these types of graphic output are readily available at
the computing facility of the National Center for Atmospheric Research in
Boulder, CO, where this model was developed. However, they are generally not
transportable to other computing facilities, and thus were not incorporated in
this model.

The model in its present form includes a tabular output of several variables.
If graphics are not available, the user may find it useful to add other variables,
or delete some of those already included, depending on the needs of each
particular application.

New page

SECTION 11 - BIBLIOGRAPHY

Alofs, D. F., and J. C. Carstens, 1976: Numerical simulation of a widely used cloud nucleus counter. J. Appl. Meteor., 15, pp. 353-354.

Arnason, G., and P.S. Brown, Jr., 1971: Growth of Cloud Droplets by Condensation: A Problem in Computational Stability. J. Atmos. Sci., 28, pp. 72-77.

Bird, R. B., W. E. Stewart, and E. N. Lightfoot, 1960: Transport Phenomena. Wiley, New York.

Carstens, J. C. and J. L. Kassner, Jr., 1968: Some aspects of droplet growth theory applicable to nuclei measurements. J. Rech. Atmos., 3, pp. 33-39.

Dahl, O. J., E. W. Dijkstra, and C. A. R. Hoare, 1972: Structured Programming. Academic Press, New York.

Davies, C. N., 1966: Aerosol Science. Academic Press, New York.

Davis, M. H., 1976: Preliminary analysis and discussion of the ground based scientific functional simulator for the ACPL. USRA, Boulder, Colorado.

Fletcher, N. H., 1962: The Physics of Rainclouds. Cambridge University Press, London.

Fuchs, N. A., 1964: The Mechanics of Aerosols. McMillan, New York.

Fukuta, N., and L. A. Walter, 1970: Kinetics of hydrometeor growth from a vapor-spherical model. J. Atmos. Sci., 27, pp. 1160-1172.

Hidy, G. M., and J. R. Brock, 1970: The Dynamics of Aerocolloidal Systems. Pergamon, New York.

Hirschfelder, J. O., C. F. Curtiss, and R. B. Bird, 1964: Molecular Theory of Gases and Liquids. Wiley, New York.

Katz, J. L., and P. Mirabel, 1975: Calculation of supersaturation profiles in thermal diffusion cloud chambers. J. Atmos. Sci., 32, pp. 646-652.

Lapidus, L. and J.H. Seinfeld, 1971: Numerical Solution of Ordinary Differential Equations. Academic Press, New York.

Ledgard, H. F., 1975: Programming Proverbs for Fortran Programmers. Hayden, Rochelle Park, New Jersey.

Lopez, M. E., 1972: Optimization of some computational procedures in orographic precipitation models. Report to U. S. Bureau of Reclamation, Division of Atmospheric Water Resources Management.

Mason, B. J., 1971: The Physics of Clouds. Oxford, London.

Marrero, T. R., and E. A. Mason, 1972: Gaseous diffusion coefficients. J. Phys. Chem. Ref. Data, 1, pp. 3-118.

McGowan, C. L., and J. R. Kelly, 1975: Top-Down Structured Programming Techniques. Petrocelli-Charter, New York.

Nix, N., and N. Fukuta, 1973: Nonsteady-state theory of droplet growth. J. Chem. Phys., 58, pp. 1735-1740.

Squires, P., 1952: The growth of cloud drops by condensation. Aust. J. Scient. Res. A5, p. 59.

Wirth, N., 1971: Program development by successive refinement. Comm. ACM, 14.

Young, K. C., 1974: A numerical simulation of winter-time, orographic precipitation. Part I. Description of model microphysics and numerical techniques. J. Atmos. Sci., 31, pp. 1735-1748.

New page

APPENDIX E - CFD FLUID DYNAMICS

INTRODUCTION

The fluid dynamics of the continuous flow diffusion chamber have been examined using two-dimensional models as a first approximation. The CFD chamber, shown in Figure E-1, consists of an elliptical cylinder between two parallel plates. The center third of the cylinder serves as an injection manifold for the aerosol laden flow. The flow exists the chamber through the three exit ports at the right edge of Figure E-1. The center exit port is used to extract the aerosol laden flow while the outside exit ports are used to extract as much of the sheath flow as possible.

Separate two-dimensional models have been developed to approximate the flow in the central vertical plane (X=0) and the central horizontal plane (Y=0). The models do not allow for the transfer of momentum from plane to plane and therefore they do not give a complete picture of the fluid dynamics. A three-dimensional calculation is required to obtain the fluid dynamics of the CFD. The fluid models ignore the temperature differential between the two flat plates in the chamber and were designed at a time when only one exit port was planned for the CFD.

FORMULATION OF THE PROBLEM

The geometry of the model used to describe the vertical problem is shown in Figure E-2 and that of the horizontal problem is shown in Figure E-3. In both models a uniform flow enters the chamber with only a Z component of velocity at Z=0. At the downstream end of the chamber, a parabolic velocity profile (Poiseuille flow) is assumed to have developed. The length of the exit port is checked to insure a Poiseuille flow will develop in the exit port.

The following derivation of the relevant fluid equations are for the vertical plane (X=0) model, but they may easily be transposed to the horizontal plane (Y=0) model. The steady flow of an incompressible viscous fluid is described by the steady-state continuity equation

$$\frac{\partial V}{\partial Y} + \frac{\partial W}{\partial Z} = 0 \qquad\qquad \text{(E-1)}$$

and the steady-state Navier-Stokes equations

$$V \frac{\partial V}{\partial Y} + W \frac{\partial V}{\partial Z} = \frac{-1}{\rho} \frac{\partial P}{\partial Y} + \nu \left(\frac{\partial^2}{\partial Y^2} + \frac{\partial^2}{\partial Z^2} \right) V \qquad (E-2)$$

$$V \frac{\partial W}{\partial Y} + W \frac{\partial W}{\partial Z} = \frac{-1}{\rho} \frac{\partial P}{\partial Z} + \nu \left(\frac{\partial^2}{\partial Y^2} + \frac{\partial^2}{\partial Z^2} \right) W \qquad (E-3)$$

where V and W are the Y and Z components of velocity, P is the pressure, ρ is the fluid density, and ν is the kinematic visiosity. By introducing a stream function ψ defined

$$V = - \frac{\partial \psi}{\partial Z}$$

$$W = \frac{\partial \psi}{\partial Y}$$

and eliminating the pressure term in Equations (E-2) and (E-3), a fourth order equation is obtained

$$\left(\frac{\partial \psi}{\partial Y} \frac{\partial}{\partial Z} - \frac{\partial \psi}{\partial Z} \frac{\partial}{\partial Y} \right) \left(\frac{\partial^2}{\partial Y^2} + \frac{\partial^2}{\partial Z^2} \right) \psi = \nu \left(\frac{\partial^2}{\partial Y^2} + \frac{\partial^2}{\partial Z^2} \right) \psi \qquad (E-4)$$

The vorticity $\bar{\Omega}$ is defined as the curl of the velocity. In this case the only non-zero component of $\bar{\Omega}$ lies along the X-axis (Y-axis in the horizontal model) and is designated Ω.

$$\Omega = \frac{\partial W}{\partial Y} - \frac{\partial V}{\partial Z} = - \left(\frac{\partial^2}{\partial Y^2} + \frac{\partial^2}{\partial Z^2} \right) \psi \qquad (E-5)$$

Substitution of Equation (E-5) in Equation (E-4) yields the vorticity transport equation

$$\frac{\partial \psi}{\partial Z} \frac{\partial \Omega}{\partial Y} - \frac{\partial \psi}{\partial Y} \frac{\partial \Omega}{\partial Z} = \nu \left(\frac{\partial^2}{\partial Y^2} + \frac{\partial^2}{\partial Z^2} \right) \Omega \qquad (E-6)$$

Supersedes page E-2, original issue

At all points other than the inlet to the parallel plates (Z=0) and the throat inlet (vertical model only) the vorticity may be calculated from Equation (E-5). The inlet vorticity may be calculated by expanding the stream function in a Taylor series about the inlet point (Z=α).

$$\psi_{(Y,\delta)} = \psi_{(Y,\alpha)} + (\delta - \alpha) \left(\frac{\partial \psi}{\partial Z} \right)_{Z=\alpha} + \frac{1}{2} (\delta - \alpha)^2 \left(\frac{\partial^2 \psi}{\partial Z^2} \right)_{Z=\alpha}$$

$$+ \frac{1}{6} (\delta - \alpha)^3 \left(\frac{\partial^3 \psi}{\partial Z^2} \right)_{Z=\alpha} \tag{E-7}$$

By using Equation (E-5) to evaluate the higher order partial derivative in Equation (E-7), the vorticity at the inlets may be written in a form which allows for the upstream diffusion of vorticity.

$$\Omega(Y,\alpha) = \frac{-1}{2} \Omega(Y,\delta) - \frac{3}{(\delta-\alpha)^2} \left(\psi_{(Y,\delta)} - \psi_{(Y,\alpha)} \right) - \frac{1}{2} \left(\frac{\partial^2 \psi}{\partial Y^2} \right)_{Z=\alpha} \tag{E-8}$$

Because Equation (E-4) is an elliptic equation, boundary conditions must be specified on all boundaries. The boundary conditions of each model will be discussed individually. Using Figure E-2 the vertical model describes the flow past an elliptical injection manifold located between two parallel plates. The injection of an aerosol laden fluid and the effects of the exit port are included in the calculation. The inlet flow (Z=0) is assumed to be uniform. A no-slip boundary condition (fluid velocity at the surface is equal to zero) is employed at every solid surface. The aerosol laden flow originates at the throat inlet as a uniform flow with flow rate to be specified independently of the main flow rate. The length of the exit port is chosen to insure that a parabolic velocity profile is present at the downstream boundary of the exit port. The calculation takes advantage of the natural symmetry of the CFD about the plane Y=0 by only considering the upper half plane in Figure E-2. The centerline boundary requires a zero Y-component of velocity and $\frac{\partial W}{\partial Y} = 0$ on the centerline Y = 0.

Supersedes page E-3, original issue

The horizontal plane problem also uses uniform flow and Poiseuille flow as the upstream and downstream boundary conditions, respectively. However, the inlet is taken downstream of the injection manifold. A no-slip boundary condition is employed at Z=CLEN (see Figure E-3) on the wall which constricts the flow into the exit port. Using symmetry the calculation only needs to consider the upper half plane in Figure E-3. The centerline (X=0) boundary condition is U=0 and $\frac{\partial W}{\partial X}$ = 0 where U is the X-component of the fluid velocity. Either a no-slip or a uniform flow boundary condition may be used on the boundary at X=CWID/2. A no-slip boundary condition implies a solid surface while a uniform flow boundary condition (U=0, W=<W> , where <W> is the average Z-component of velocity for any X<CLEN) simulates a flow with moving boundaries as in the case of three exit ports. The exit port wall is considered a solid boundary necessitating a no-slip boundary condition in all cases.

METHOD OF SOLUTION

An iterative method was used to obtain a solution of the finite difference forms of Equations (E-5) and (E-6). The derivatives at all interior points were expressed in center-difference form using nearest-neighbor points on a rectangular grid. A nested grid was used downstream of the injection manifold in the vertical model. The dimensions of the elliptical cylinder were chosen to insure that the locus of points forming the ellipse coincided with the rectangular grid. Equations (E-5) and (E-6) were iterated separately using a Gauss-Seidel iteration. The overrelaxation technique was only applied to the stream function iteration. A complete iteration consisted of an iteration of the vorticity using Equation (E-8) at the inlet and Equation (E-6) at every other grid point followed by an iteration of the stream function using Equation (E-5) at every interior point. The boundary conditions were maintained by not iterating the values of the stream functions on the boundaries.

The value of the relaxation coefficient (RELAX) has to be determined by trial and error and usually is in the interval from 1.00 to 1.40. Convergence is achieved when the maximum change in the stream function at any grid point was less than a specified value (CONCRT) usually 1.0×10^{-6}. Once the calculation converged, final values of the velocity components and the vorticity were calculated from center-difference formulas.

Supersedes page E-4, original issue

RESULTS

Streamlines are shown in Figures E-4 and E-5 for a typical CFD geometry with carrier and aerosol laden flows corresponding to Reynolds numbers of 14.3 and 3.6 respectively. The size and shape of the injection manifold has been varied to observe any effects on the streamlines. A pocket of reverse flow appears in the upper corner of the CFD above the exit port. The carrier flow remains laminar throughout the length of the CFD and does not separate from the injection manifold. The thickness of the aerosol stream can be measured at any point downstream of the injection manifold. The convergence of the combined flow can be seen as it approaches the exit port. This model ignores the transfer of momentum to the central vertical plane as the fluid exits the chamber.

Streamlines obtained using the horizontal model are shown in Figure E-6. Figure E-6a illustrates the uniform flow boundary condition while Figure E-6b corresponds to the no-slip boundary condition. As with the previous model, the momentum transfer to and from the plane of the model is ignored. With the no-slip boundary condition, the fluid will develop the parabolic velocity profile corresponding to a viscous incompressible flow between two parallel plates. As the flow nears the exit port, the fluid along the centerline slows down in the no-slip case only. The uniform flow case does not allow for deceleration of the centerline fluid. Using the horizontal model, it is possible to calculate the time spent in any section of the chamber along any streamline.

Even though the horizontal plane does not include the elliptical injection manifold, generalizations about the behavior of the aerosol laden flow in the central horizontal plane (Y=0) can be made. Use of the vertical model without a sheath flow shows that the aerosol laden flow develops a parabolic shape as it spreads out from the diffuser to the walls of the chamber. Similar behavior in the horizontal plane can be expected in the absence of a sheath flow. In the presence of a sheath flow, the aerosol laden flow will spread out as it exits the manifold but will be stopped by the sheath flow returning to the central horizontal plane before it (the aerosol laden flow) reaches the vicinity of the wall. The extent of the spreading of the

Supersedes page E-5, original issue

aerosol laden flow can only be determined with a full three-dimensional analysis of the CFD including flow around the elliptical injection manifold as well as exit flow.

CONCLUSIONS

Both vertical and horizontal plane models are operational but do not include momentun transfer to and from the plane of the model. Therefore, the models give only a first approximation to the CFD fluid dynamics.

Both models include a test to see if the exit port is long enough for a Poiseuille flow to form in the exit length. If this condition is not fulfilled, the calculation would diverge. To save computer resources, the calculation is terminated after a suggested exit length is calculated.

The speed at which convergence is reached and to some extent whether or not convergence is possible depends on the value of the relaxation coefficient. Not much is known about the relatioship other than trial and error methods suggest a value of between 1.0 and 1.4 for the vertical plane model. If the relaxation coefficient is greater (less) than one the procedure is said to be overrelaxed (underrelaxed). When working with high velocity (>1.5 cm/sec) it is probably best to underrelax the horizontal calculations.
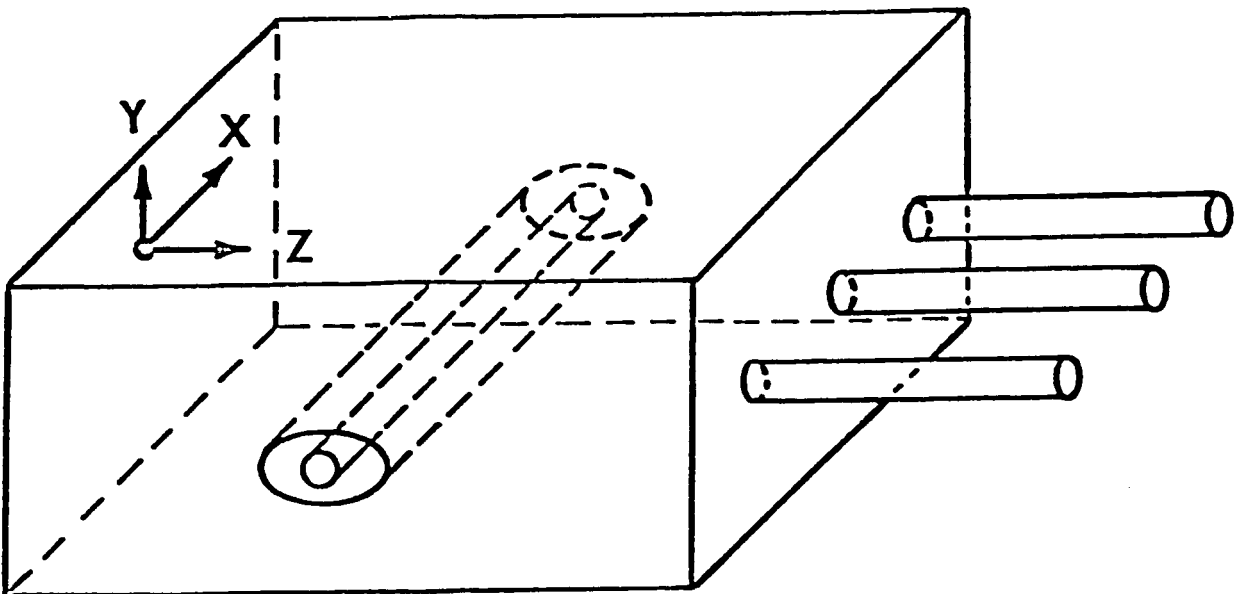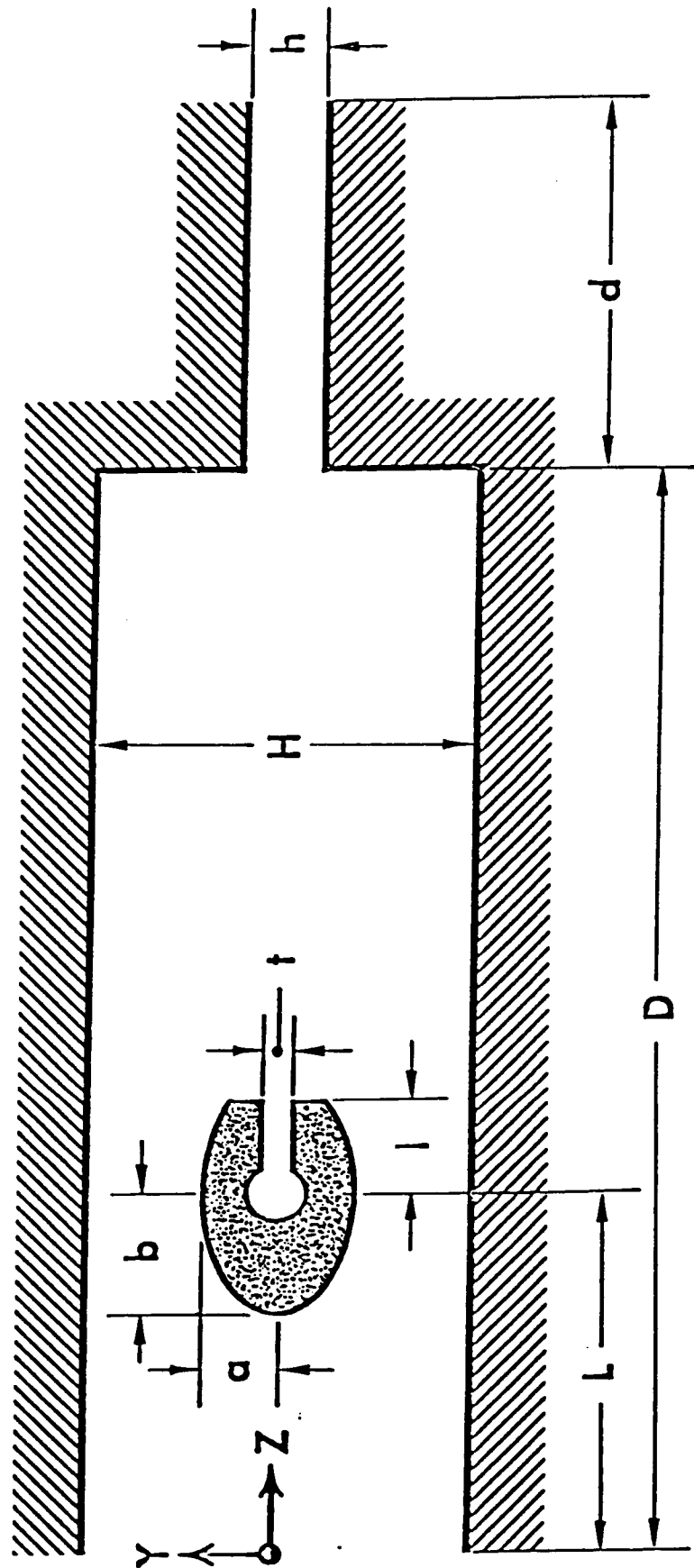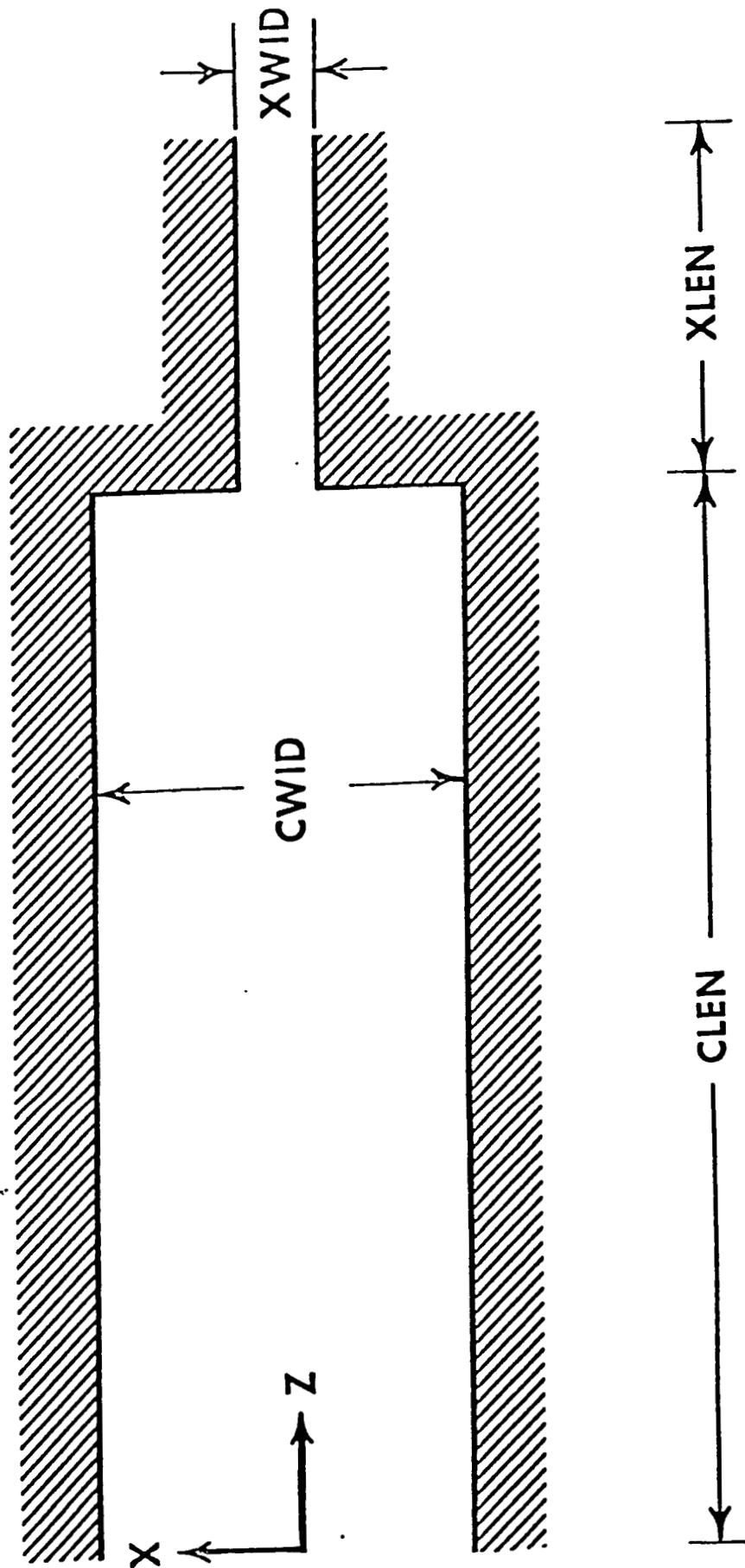
Supersedes page E-6, original issue

Figure E-1. Three Exit Port Chamber

VERTICAL PLANE (X=O)

Figure E-2. Vertical Plane Geometry

XWID

XLEN

CWID

CLEN

Z

X

HORIZONTAL PLANE (Y=O)

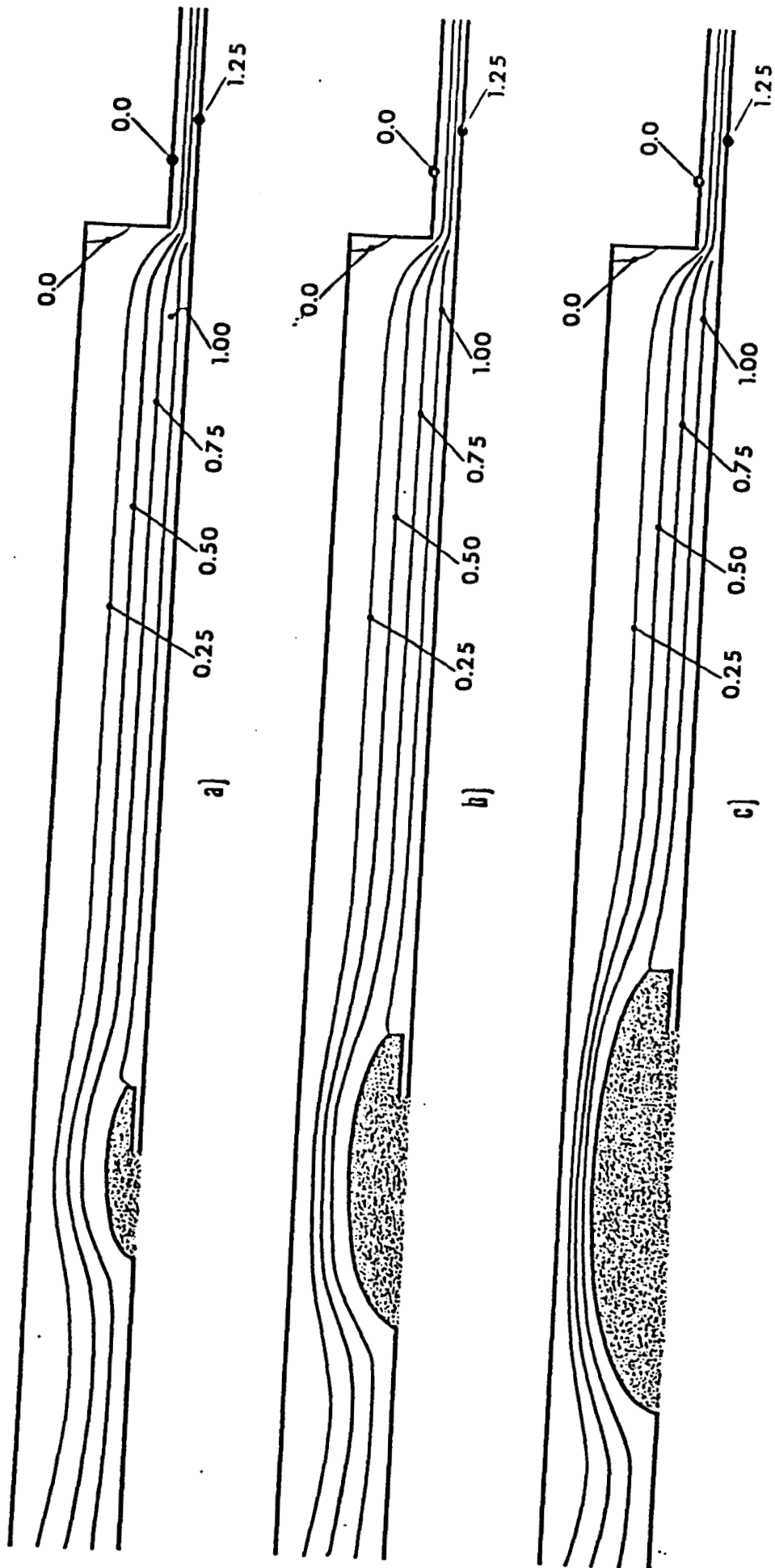Figure E-3. Horizontal Plane Geometry

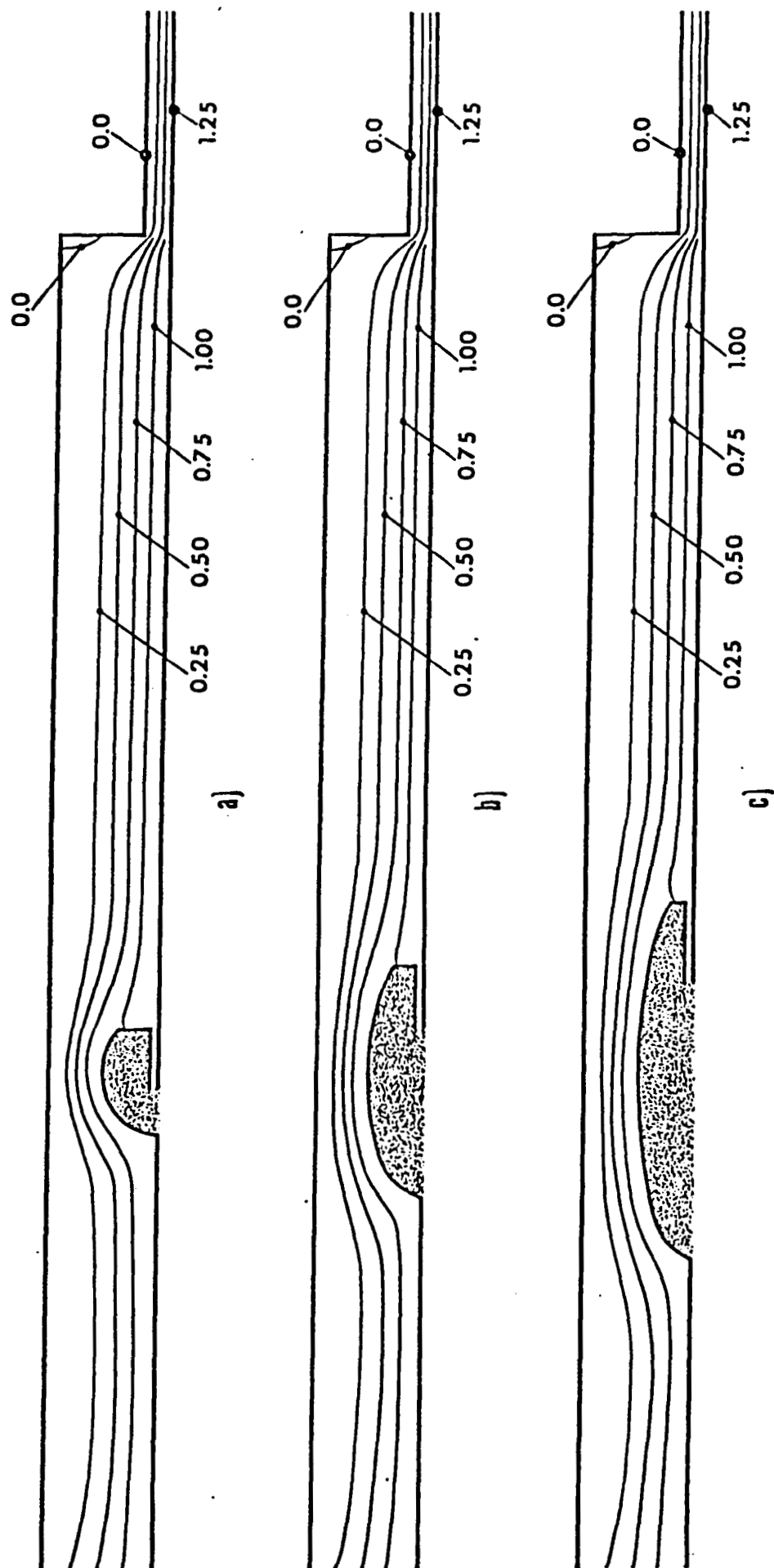Figure E-4. Typical CFD Geometry, Reynolds Number 14.3
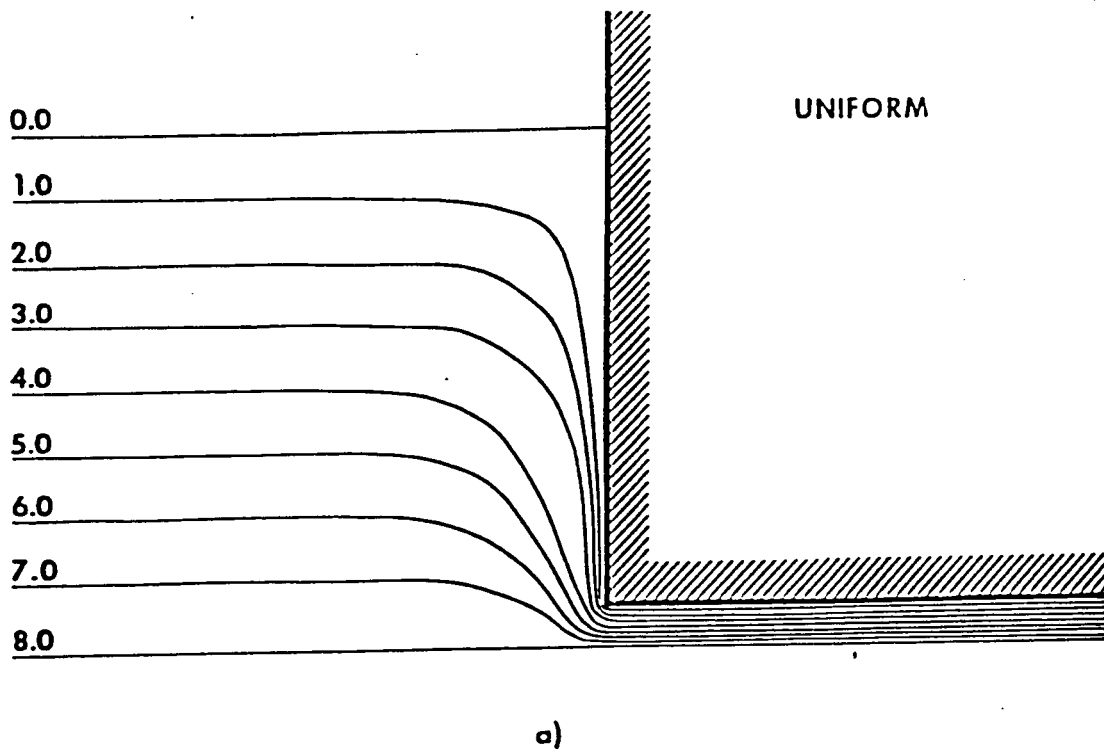
Figure E-5. Typical CFD Geometry, Reynolds Number 3.6
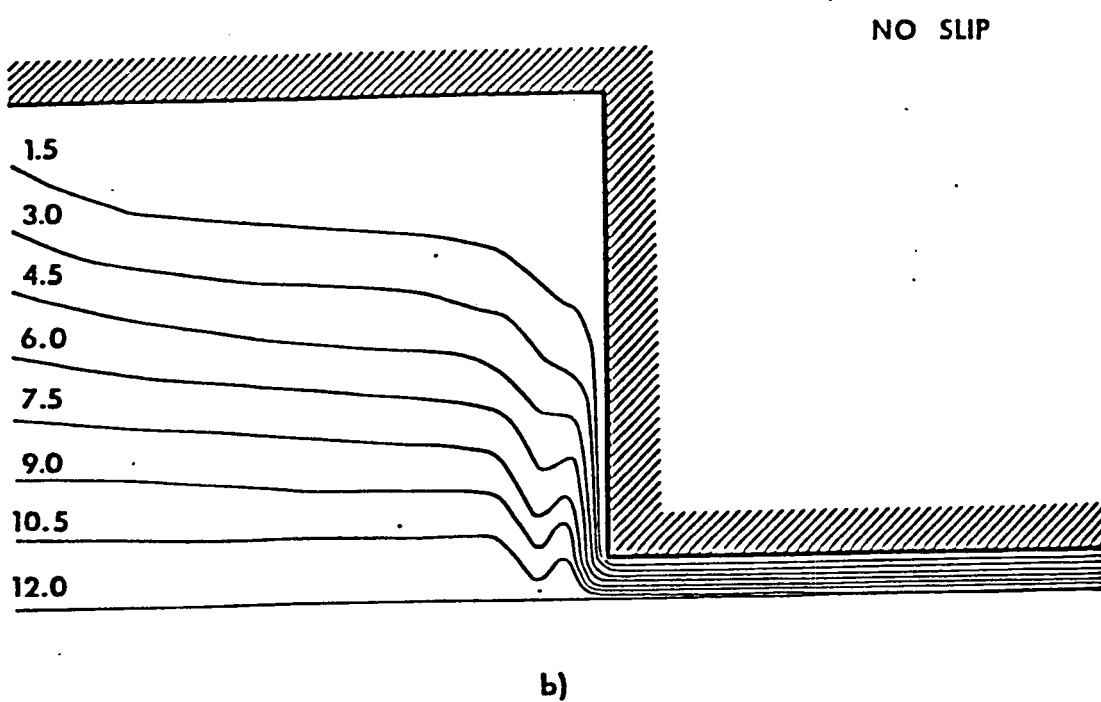
New page

a)

Figure E-6a. Uniform Flow Boundary Condition

b)

Figure E-6b. No-Slip Boundary Condition

New page

APPENDIX F - CS^k AEROSOL DISTRIBUTION

The aerosol characterization considered here is in terms of its cumulative number distribution as a function of the critical supersaturation. This distribution can be expressed as

$$N = CS^k$$

where

     N = cumulative or total number of aerosol particles per CC

     C = a constant

     k = value of exponent k in the distribution

     S = critical supersaturation

This expression generates a discrete distribution with N total particles per CC, obeying the CS^k distribution between S_{min} and S_{max}, and with no particles with critical supersaturations outside of this range. For different values of k,
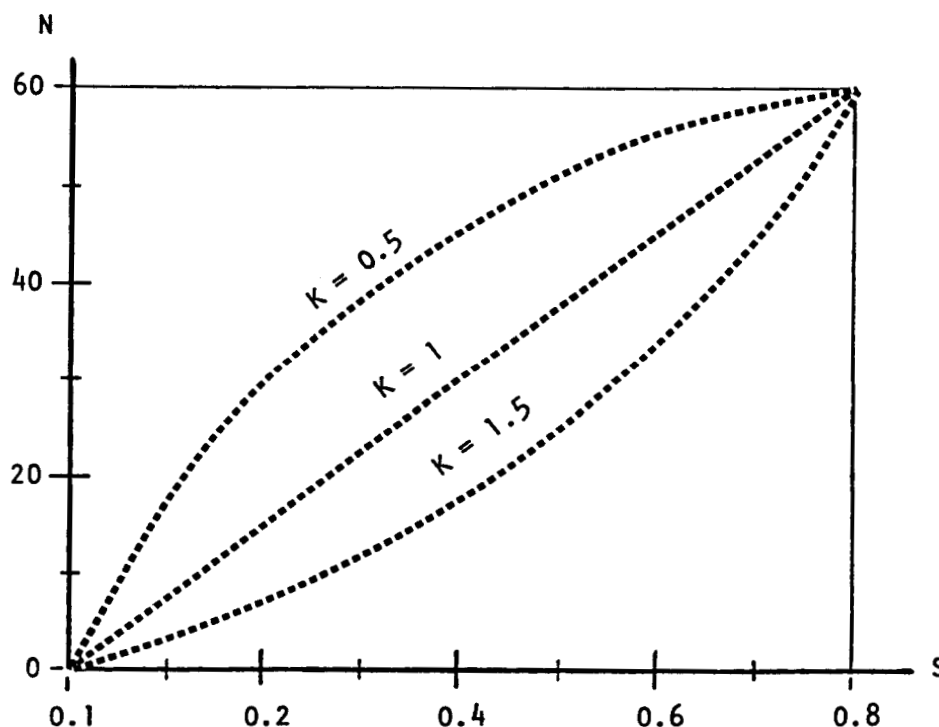

Figure F-1 - Samples of CS^k Distribution

New page

the cumulation distribution functions N are shown in Figure F-1. To use this distribution function, one needs the following input data:

N = total or cumulative number of aerosol particles per CC

K = exponential value

S_{min} = minimum critical supersaturation

S_{max} = maximum critical supersaturation

With the given data, one can compute the following parameters:

$$C = \frac{N}{\left[S_{max}^k - S_{min}^k\right]}$$

$$N_0 = C * S_{min}^k$$

$$\Delta N = \frac{N}{\text{No. of Classes}}$$

and

$$S(I) = \left[\frac{(I * \Delta N + N_0)}{C}\right]^{1/K}$$

$$NZ(I) = \Delta N$$

where $I = 1, 2, 3, \text{---------} $ No. of aerosol classes.

The capability for computing the CS^k Aerosol Distribution was implemented as an input processing for the ACPL Simulator System.

New page

APPENDIX G - THREE DIMENSIONAL ANALYSIS OF THE EXIT FLOW
OF A CFD WITH A SINGLE EXIT PORT

INTRODUCTION

The method of solution is based on the results of Briley (1) for predicting flows in rectangular ducts. Since the CFD narrows into an exit port, Briley's method must be extensively modified. Briley (1) used the approximate Navier-Stokes equations, having discarded the streamwise convection terms. In the present calculation, the streamwise term is important in the region of the exit port and must be retained. An inviscid pressure approximation is used to calculate the axial velocity and a viscous pressure or pressure fluctuation is used to balance the continuity equation.

FORMULATION OF THE PROBLEM

The geometry of the problem is shown in Figure 1. The CFD is approximated by a rectangular duct which terminates into a smaller rectangular exit duct. The aspect ratios of the two ducts need not be the same. A three-dimensional orthogonal grid system is used over the combined chamber and exit port. The grid spacing is determined by the size of the chamber and the number of grid points. The size of the exit duct must then be adjusted to fit the grid. The origin of the coordinate system is chosen on the axis of the chamber and the X- and Y- axes normal to the sides of the chamber.

The governing equations are the Navier-Stokes and continuity equations written in Cartesian coordinates with the primary flow in the Z-direction and secondary flow in the XY-plane. The Navier-Stokes equations can be written as

$$U\frac{\partial W}{\partial X} + V\frac{\partial W}{\partial Y} + W\frac{\partial W}{\partial Z} = -\frac{1}{\rho}\frac{\partial}{\partial Z}(P + p) + \nu(\frac{\partial^2 W}{\partial X^2} + \frac{\partial^2 W}{\partial Y^2} + \frac{\partial^2 W}{\partial Z^2}) \qquad (1)$$

$$U\frac{\partial V}{\partial X} + V\frac{\partial V}{\partial Y} + W\frac{\partial V}{\partial Z} = -\frac{1}{\rho}\frac{\partial p}{\partial Y} + \nu(\frac{\partial^2 V}{\partial X^2} + \frac{\partial^2 V}{\partial Y^2} + \frac{\partial^2 V}{\partial Z^2}) \qquad (2)$$

$$U\frac{\partial U}{\partial X} + V\frac{\partial U}{\partial Y} + W\frac{\partial U}{\partial Z} = -\frac{1}{\rho}\frac{\partial p}{\partial X} + \nu(\frac{\partial^2 U}{\partial X^2} + \frac{\partial^2 U}{\partial Y^2} \quad \frac{\partial^2 U}{\partial Z^2}) \qquad (3)$$

where U, V, and W are the X, Y, and Z components of the velocity, $\overline{q}$, P is the inviscid pressure, p is a viscous pressure correction, ν the kinematic viscosity, and ρ is the density. The continuity equation is used as a fourth equation.
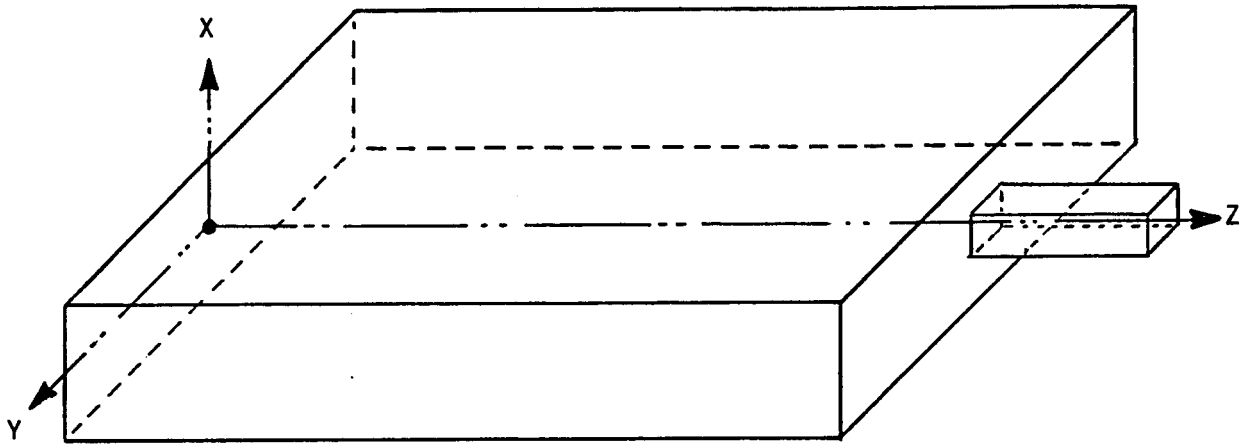
New page

G-2

FIGURE 1. GEOMETRY USED TO CALCULATE THREE DIMENSIONAL EXIT FLOW

New page

$$\frac{\partial U}{\partial X} + \frac{\partial V}{\partial Y} + \frac{\partial W}{\partial Z} = 0 \tag{4}$$

As there are 5 variables in Equations (1) to (4), U, V, W, P, and p, a fifth equation,

$$\iint\limits_{\substack{\text{duct} \\ \text{cross-section}}} w \, dxdy = \frac{\dot{m}}{\rho}, \tag{5}$$

where $\dot{m}$ is the mass flow rate, a constant determined by the initial condition, will be used to complete the set of 5 equations in 5 variables.

Briley (1) has ignored the streamwise diffusion of all three velocity components by dropping all second order derivatives with respect to Z. The inviscid pressure P is assumed known from a potential flow solution and the components of its gradient are treated as source terms. In the case of a straight duct, the potential flow with constant axial velocity and pressure is used, P is constant and therefore, its gradient is zero. As suggested by Patankar and Spalding (2), the viscous pressure correction p, in the primary flow equation (1), is treated separately from that in the secondary flow equations (2) and (3). In equation (1), the $\frac{\partial p}{\partial Z}$ term is redefined to mean a viscous pressure drop which is a function of Z only and is computed as part of the solution using equation (5). Thus, $\frac{\partial p}{\partial Z}$ is replaced by $\frac{dp_m(Z)}{dZ}$. In the secondary flow equations, p is required to vary in the XY-plane in such a way as to insure that the continuity equation (4) is satisfied at every point.

METHOD OF SOLUTION

The method used to solve the set of equations will be described in this section. All of the equations are expressed in finite-difference form. In general terms, the method is as follows for each XY-plane.

New page

1) W is computed from the Z-component of the Navier-Stokes equation, equation (1) with p_m determined implicitly to insure that the axial mass flow equation (5) is satisfied.

2) U and V are approximated by U_p and V_p, predictions computed from the transverse momentum equations. Small corrections, U_c and V_c, are then computed to satisfy the continuity equation (4).

3) p is computed from a Poisson equation for pressure, computed from the transverse Navier-Stokes equations which are evaluated using the corrected values for U and V.

The Z component of the velocity is computed by iterating the Z component of the Navier-Stokes equation using a Jacoby iteration and the pressure p_m using a secant iteration. The pressure drop term was expanded using an upstream differencing technique

$$\frac{d}{dZ} p_m(Z) = (p_m(L) - p_m(L-1))/\Delta Z$$

where L is the index on the Z-grid beginning at the origin.

Since $p_m(L)$ is initially unknown, the correct value is obtained implicitly using the standard secant iteration technique. The basic procedure can be summed up as

1) assume a value for $p_m(L)$,
2) solve equation (1) for the axial flow field using a Jacoby iteration, and
3) compute the mass flow.

A no-slip boundary condition was used for values of W on the walls of the chamber and exit port.

The transverse velocities are decomposed using the following relations.

$$U = U_p + U_c \tag{6}$$
$$V = V_p + V_c \tag{7}$$

where U_p and V_p are predictions of U and V obtained from the transverse momentum equations and U_c and V_c are corrections to U_p and V_p of first order in ΔZ. The velocity predictions are obtained from a Gauss-Seidel iteration of

New page

the transverse Navier-Stokes equations. The boundary conditions require U_p and V_p to be zero at the walls.

The corrections are of order ΔZ and may be obtained from the result of substituting equations (6) and (7) in equation (9).

$$\frac{\partial U}{\partial X} + \frac{\partial V}{\partial Y} = (\frac{\partial U_p}{\partial X} + \frac{\partial U_c}{\partial X}) + (\frac{\partial V_p}{\partial Y} + \frac{\partial V_c}{\partial Y}) = -\frac{\partial W}{\partial Z} \tag{8}$$

Next, it is assumed that the corrections are irrotational, and may be described by a velocity potential ϕ such that

$$U_c = \frac{\partial \phi}{\partial X} \tag{9}$$

$$V_c = \frac{\partial \phi}{\partial Y} \tag{10}$$

A Poisson equation for the velocity potential is obtained by substituting equations (9) and (10) in equation (8).

$$(\frac{\partial^2}{\partial X^2} + \frac{\partial^2}{\partial Y^2}) \phi = -\left[\frac{\partial U_p}{\partial X} + \frac{\partial V_p}{\partial Y} + \frac{\partial W}{\partial Z}\right] \tag{11}$$

Since the values of U_p, V_p, and W do not exist at points outside the wall, one-sided derivatives are used on the walls. The boundary condition requires the normal derivative of ϕ to vanish. Once ϕ is known, U_c and V_c are known by definition and U and V are computed from equations (6) and (7). In general the no-slip boundary conditions on U_c and V_c are not satisfied, since only one component of the velocity correction can be specified on the walls. The no-slip condition is satisfied to first order in ΔZ since U_c and V_c are first order corrections to U_p and V_p which do satisfy the no-slip boundary condition.

Once U and V have been computed, values of the viscous pressure correction may be calculated. Differenced forms of the transverse Navier-Stokes equations are evaluated using the newly computed values of U and V.

New page

$$T_1 = \frac{\partial p}{\partial X} = -\rho \left[U\frac{\partial U}{\partial X} + V\frac{\partial U}{\partial Y} + W\frac{\partial U}{\partial Z} - \nu(\frac{\partial^2 U}{\partial X^2} + \frac{\partial^2 U}{\partial Y^2} + \frac{\partial^2 U}{\partial Z^2}) \right] \qquad (12)$$

$$T_2 = \frac{\partial p}{\partial Y} = -\rho \left[U\frac{\partial V}{\partial X} + V\frac{\partial V}{\partial Y} + W\frac{\partial V}{\partial Z} - \nu(\frac{\partial^2 V}{\partial X^2} + \frac{\partial^2 V}{\partial Y^2} + \frac{\partial^2 V}{\partial Z^2}) \right] \qquad (13)$$

A Poisson equation for p is obtained by differentiation of equations (12) and (13).

$$(\frac{\partial^2}{\partial X^2} + \frac{\partial^2}{\partial Y^2}) \, p = -(\frac{\partial T_1}{\partial X} + \frac{\partial T_2}{\partial Y}) \qquad (14)$$

Equation (14) has the same form as equation (11) and was also solved using a Gauss-Seidel iterative technique. The quantities T_1 and T_2 can be evaluated everywhere except on the walls and therefore, equation (14) is solved in the region bounded by the rows of grid points, and the value of the pressure fluctuation on the wall is found from the boundary condition at the computational boundary.

ITERATION PROCEDURE

The procedure developed by Briley marched down the duct in the Z-direction once, calculating the complete set of variables U, V, W, P, and p for each XY-plane. The difference formulas have been manipulated such that values at the (L+1)st level of the Z index are calculated using the Lth level values. Such a procedure, known as upstream or backwards differencing allows the entire flow field to be calculated with one pass of the duct.

Such a procedure must be modified in the core of the CFD model developed in the previous section due to the importance of streamwise diffusion near the exit port. The method used for the CFD model employed center-difference formulas and an iteration on the Z-direction as well as iterations in the XY-plane. Five separate convergence criteria must be supplied for 1) W, 2) P, 3) U_p and V_p, 4) ϕ, and 5) p. The same criteria was used for W, the Z-component of velocity, and U_p and V_p, the predictions of the transverse velocities. Similarly both pressure variables, P and p, are compared to the same pressure tolerance. A separate criterion was used to check the convergence of the velocity potential.

New page

Since the main area of interest is the exit region, the computation time may be decreased by assuming a semi-developed flow at the first grid point. This is achieved at the beginning of each large iteration by setting the Z-component of velocity at every point in the first six (6) XY planes equal to the value at the corresponding point of the 7th plane.

Final convergence is monitored by observing the pressure P at the downstream end of the exit port. When the relative pressure change between successive iterations was less than TOLPI, the iteration was said to have converged.

1) Briley, W. R., J. Comp. Phys. <u>14</u> 8 (1974)
2) Patankar, S. V. and Spalding, D. B. Internat, J. Heat Mass Transfer <u>15</u> 1787 (1972)

New page